The Astrophysical Journal Letters, 779:L1 (6pp), 2013 December 10 doi:10.1088/2041-8205/779/1/L1

NuSTAR OBSERVATIONS OF GRB 130427A ESTABLISH A SINGLE COMPONENT SYNCHROTRON AFTERGLOW ORIGIN FOR THE LATE OPTICAL TO MULTI-GEV EMISSION

C. Kouveliotou[1], J. Granot[2], J. L. Racusin[3], E. Bellm[4], G. Vianello[5], S. Oates[6], C. L. Fryer[7], S. E. Boggs[8], F. E. Christensen[9], W. W. Craig[8,10], C. D. Dermer[11], N. Gehrels[3], C. J. Hailey[12], F. A. Harrison[4], A. Melandri[13], J. E. McEnery[3], C. G. Mundell[14], D. K. Stern[15], G. Tagliaferri[13], and W. W. Zhang[3]

[1] Astrophysics Office/ZP12, NASA Marshall Space Flight Center, Huntsville, AL 35812, USA; chryssa.kouveliotou@nasa.gov
[2] Department of Natural Sciences, The Open University of Israel, 1 University Road, P.O. Box 808, Ra'anana 43537, Israel; granot@openu.ac.il
[3] NASA Goddard Space Flight Center, Greenbelt, MD 20771, USA; judith.racusin@nasa.gov
[4] Cahill Center for Astronomy and Astrophysics, California Institute of Technology, 1200 E. California Blvd., Pasadena, CA 91125, USA
[5] W. Hansen Experimental Physics Laboratory, Kavli Institute for Particle Astrophysics and Cosmology, Department of Physics and SLAC National Accelerator Laboratory, Stanford University, Stanford, CA 94305, USA
[6] Mullard Space Science Laboratory, University College London, Holmbury St. Mary, Dorking, Surrey RH5 6NT, UK
[7] CCS-2, Los Alamos National Laboratory, Los Alamos, NM 87545, USA
[8] Space Sciences Laboratory, University of California, Berkeley, CA 94720, USA
[9] DTU Space-National Space Institute, Technical University of Denmark, Elektrovej 327, 2800 Lyngby, Denmark
[10] Lawrence Livermore National Laboratory, Livermore, CA 94550, USA
[11] Code 7653, National Research Laboratory, Washington, DC 20375-5352, USA
[12] Columbia Astrophysics Laboratory, Columbia University, New York, NY 10027, USA
[13] INAF-Osservatorio Astronomico di Brera, via E. Bianchi 46, I-23807 Merate, Italy
[14] Astrophysics Research Institute, Liverpool John Moores University, 146 Brownlow Hill, Liverpool Science Park, Liverpool L3 5RF, UK
[15] Jet Propulsion Laboratory, California Institute of Technology, Pasadena, CA 91109, USA
Received 2013 October 15; accepted 2013 November 7; published 2013 November 21

ABSTRACT

GRB 130427A occurred in a relatively nearby galaxy; its prompt emission had the largest GRB fluence ever recorded. The afterglow of GRB 130427A was bright enough for the *Nuclear Spectroscopic Telescope ARray* (*NuSTAR*) to observe it in the 3–79 keV energy range long after its prompt emission (∼1.5 and 5 days). This range, where afterglow observations were previously not possible, bridges an important spectral gap. Combined with *Swift, Fermi*, and ground-based optical data, *NuSTAR* observations unambiguously establish a single afterglow spectral component from optical to multi-GeV energies a day after the event, which is almost certainly synchrotron radiation. Such an origin of the late-time *Fermi*/Large Area Telescope >10 GeV photons requires revisions in our understanding of collisionless relativistic shock physics.

Key words: acceleration of particles – gamma-ray burst: individual (GRB 130427A) – magnetic fields – radiation mechanisms: non-thermal – shock waves

Online-only material: color figures

1. INTRODUCTION

Gamma-ray bursts (GRBs) release within seconds to minutes more high-energy photons than any other transient phenomenon (Kouveliotou et al. 2012). Their prompt gamma-ray emission is followed by a long-lived (typically weeks to months) afterglow, visible from radio to X-rays. The afterglow emission is attributed to synchrotron radiation from relativistic electrons accelerated in the shock produced as the explosion plows into the circumstellar medium. The afterglow synchrotron origin is supported by their broadband spectra (Granot & Sari 2002; Galama et al. 1998) and polarization measurements (Covino et al. 2004).

GRB 130427A triggered the *Fermi*/Gamma-ray Burst Monitor (GBM) at 07:47:06.42 UT on 2013 April 27 (von Kienlin 2013). The intensity and hardness of the event fulfilled the criteria for an autonomous slew maneuver to place the burst within the *Fermi*/Large Area Telescope (LAT) field of view. Its exceedingly bright prompt emission was also detected by other satellites (*AGILE*: Verrecchia et al. 2013; *Konus-Wind*: Golenetskii et al. 2013; *RHESSI*: Smith et al. 2013; *Swift*: Maselli et al. 2013) and enabled multiple ground- and space-based follow-up observations, allowing for rapid accurate determination of the event location and distance at redshift $z = 0.340$ (Levan et al. 2013), as well as extensive broadband afterglow monitoring from radio to γ-rays. The extreme X-ray and γ-ray energetics of the burst are described in detail in Preece et al. (2013), Ackermann et al. (2013), and Maselli et al. (2013). The record-breaking duration of the LAT afterglow (∼0.1–100 GeV), which lasted almost a day after the GBM trigger, placed GRB 130427A at the top of the LAT GRBs in fluence (Ackermann et al. 2013).

The extreme intensity, accurate distance measurement and relative closeness of GRB 130427A, made it an ideal candidate for follow-up observations with the *Nuclear Spectroscopic Telescope ARray* (*NuSTAR*; Harrison et al. 2013). Here we describe our *NuSTAR* afterglow observations taken during two epochs (Section 2), combined with data from *Fermi*/LAT, *Swift*, and optical observatories. We describe in Section 3 the derivation of the *Fermi*/LAT extrapolation and upper limits (ULs) during the *NuSTAR* epochs. In Section 4 we present afterglow multi-wavelength fits, and discuss our results in Section 5.

2. *NuSTAR* OBSERVATIONS

NuSTAR was launched on 2012 June 13; the instrument's two telescopes utilize a new generation of hard X-ray optics and detectors to focus X-rays in the range 3–79 keV. We observed GRB 130427A at three epochs, starting approximately 1.2, 4.8, and 5.4 days after the GBM trigger, for 30.5, 21.2, and 12.3 ks (live times). We detected the source in all epochs, obtaining for the first time X-ray observations of a GRB afterglow above 10 keV. The *NuSTAR* data thus provide an important

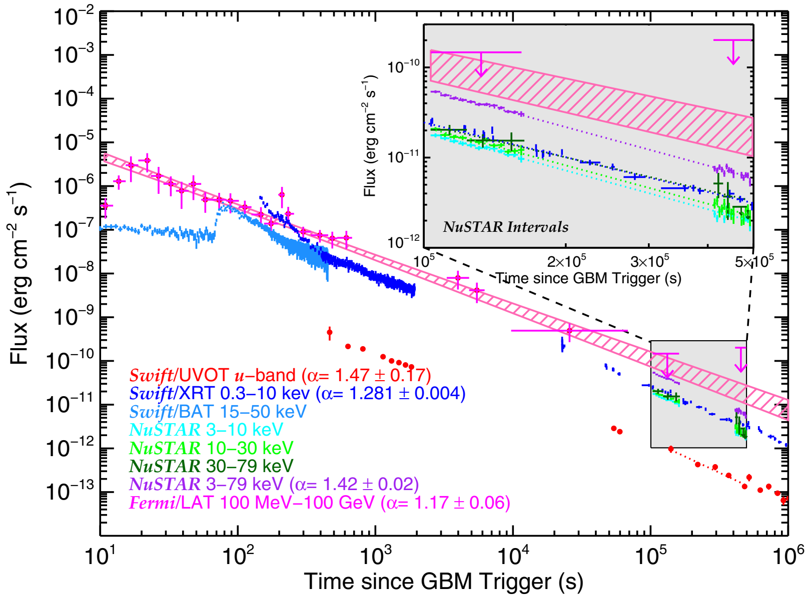

Figure 1. Light curves of GRB 130427A. (Maselli et al. 2013; Ackermann et al. 2013). All errors are 1σ. The inset zooms in on the *NuSTAR* epochs. The LAT ULs are shown as arrows and the LAT extrapolated region as a shaded rectangle (1σ). Numbers in parentheses are indices of power-law fits during the *NuSTAR* epochs.
(A color version of this figure is available in the online journal.)

missing spectral link between the *Swift*/X-Ray Telescope (XRT) observations (0.3 – 10 keV; Maselli et al. 2013) and the *Fermi*/LAT observations (>100 MeV; Ackermann et al. 2013).

We processed the data with *HEASOFT* 6.13 and the *NuSTAR* Data Analysis Software (NuSTARDAS) v. 1.1.1 using CALDB version 20130509. We extracted source light curves and spectra from circular regions with 75″ radius from both *NuSTAR* modules for the first epoch and 50″ radius for the second and third epochs. We used circular background regions (of 150″, 100″, and 100″ radius for each epoch, respectively) located on the same *NuSTAR* detector as the GRB. Hereafter, we combine the second and third *NuSTAR* epochs, which were very close in time, to increase the signal-to-noise ratio, and refer to it as the second epoch.

Figure 1 demonstrates the temporal behavior of the multi-wavelength afterglow flux of GRB 130427A. Here we have included data from *Swift*/XRT, *Swift*/Ultra-Violet/Optical Telescope (UVOT), and *Fermi*/LAT. We also include the extrapolated *Fermi*/LAT light curve derived as described in Section 3. The weighted average of the decay rates during the two *NuSTAR* epochs (single power-law (PL) fits) is $\alpha = 1.3$ from optical to GeV (see also the figure inset, and the indices next to each instrument in Figure 1). We discuss the implications of the temporal results in Section 5.

3. *Fermi* OBSERVATIONS

The *Fermi*/LAT detected GRB 130427A up to almost a day after the trigger time (Figure 1; Ackermann et al. 2013). *Fermi*/LAT was also observing during both *NuSTAR* epochs but did not detect the source. We analyzed the "Pass 7" data with the Fermi Science Tools v9r31p1 and the P7SOURCE_V6 version of the instrument response functions, and using the public Galactic diffuse model and the isotropic spectral template[16]. For each epoch, we selected all the events within a region of interest (ROI) with a radius of 10° around the position of the GRB, excluding times when any part of the ROI was at a zenith angle >100°. The latter requirement greatly reduces contamination from the diffuse gamma-ray emission originating from the Earth's upper atmosphere, peaking at a zenith angle of ∼110°.

3.1. *Fermi*/*LAT Spectra and Upper Limits*

For each epoch we performed an unbinned likelihood analysis over the whole energy range (0.1–100 GeV), using a model composed of the two background components (Galactic and isotropic) and a point source with a PL spectrum (the GRB), plus the contribution from all the known gamma-ray point sources in the ROI (Nolan et al. 2012). We did not obtain a detection in either epoch, and so we computed ULs. We froze the normalization of the background components, and fixed the photon index of the GRB model to 2.17, which is the best-fit value from the smoothly broken power-law (SBPL) fit during the first *NuSTAR* epoch as reported in Section 4 (the ULs change by less than 10% for any choice of the photon index between 2 and 2.5). We then independently fit the GRB model in three energy bands (0.1–1, 1–10, and 10–100 GeV), using an unbinned profile likelihood method to derive the corresponding 95% LAT ULs (Ackermann et al. 2012). The information contained in such ULs is important to constrain the spectrum, but cannot be handled by a standard fitting procedure. We, therefore, turn to an alternative (but equivalent) method to include the LAT observations in a broadband spectral fit. We obtained the count spectrum of the observed LAT signal (source+background) using *gtbin*, and the background spectrum using *gtbkg*, which computes the predicted counts from all the components of the best-fit likelihood model except the GRB. Since there is no significant excess above the background, the two spectra are compatible within the errors, although they are not identical. We also ran *gtrspgen* to compute the response of the instrument in the interval of interest, and loaded these files in XSPEC v.12.7. This software compares the observed net counts to the number of counts predicted by the model folded with the response of the instrument. By minimizing a statistic based on the Poisson probability, we can treat equivalently a spectrum containing a significant signal, and a spectrum which

[16] Available at http://fermi.gsfc.nasa.gov/ssc/.

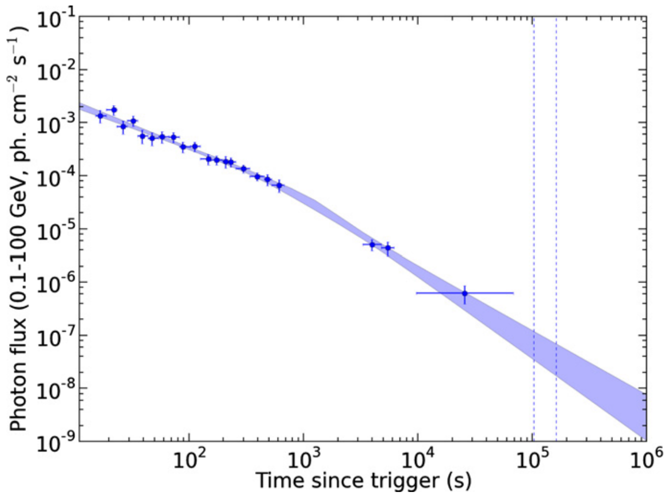

Figure 2. The decaying part of the *Fermi*/LAT photon flux light curve of the afterglow of GRB 130427A (100 MeV–100 GeV; Ackermann et al. 2013). The shaded blue region marks the 1σ contour for the best-fit BPL model, while the dashed lines indicate the start and stop times for the first *NuSTAR* epoch. Only data points used for the BPL fit (i.e., after T_0 + 16 s) are included.

(A color version of this figure is available in the online journal.)

is compatible with being just background. While the former will constrain the model to pass through the data points, the latter will constrain it to predict a number of counts above background compatible with zero. The best-fit model obtained using the LAT spectra computed in this way is, as expected, below the ULs computed with the profile likelihood method.

3.2. Extrapolation of the Fermi/LAT Light Curve

The high-energy (>100 MeV) photon and energy flux light curves are well described by a broken power law (BPL) and PL, respectively, as reported in Ackermann et al. (2013). To extrapolate such light curves to the *NuSTAR* epochs, we adopted a general approach, based on the well-known Markov Chain Monte Carlo technique, which takes into account the uncertainties on the best-fit parameters along with all their correlations, as follows.

Each data point in Figure 2 represents a photon flux derived from a likelihood fit with 1σ confidence intervals (Ackermann et al. 2013). Hence, we can assume a Gaussian joint likelihood L and minimize the corresponding $-\log(L)$ to find the best-fit parameters, which is equivalent to a standard least-squares fit (or to minimize χ^2). We can then apply the Bayes rule that the posterior distribution for the parameters is directly proportional to the prior distribution multiplied by the likelihood. If we take an uninformative prior, then the posterior distribution is directly proportional to the likelihood itself. Therefore, sampling the likelihood function with a Markov Chain Monte Carlo technique is equivalent to sampling the posterior distribution. By using, e.g., the Goodman & Weare (2010) algorithm, we can then obtain many sets of parameters distributed as in the posterior distribution, with all the relations between them taken into account. Using these sets of parameters, p_i, we can build a distribution of a certain quantity of interest $f(p_i)$. Taking the median and the relevant percentiles of the distribution, we can then extract a measure of f and its 1σ confidence interval. In this way, we computed the shaded region in Figure 2 and the expected flux only in the first *NuSTAR* epoch, which starts shortly after the last detection from *Fermi*/LAT. The second

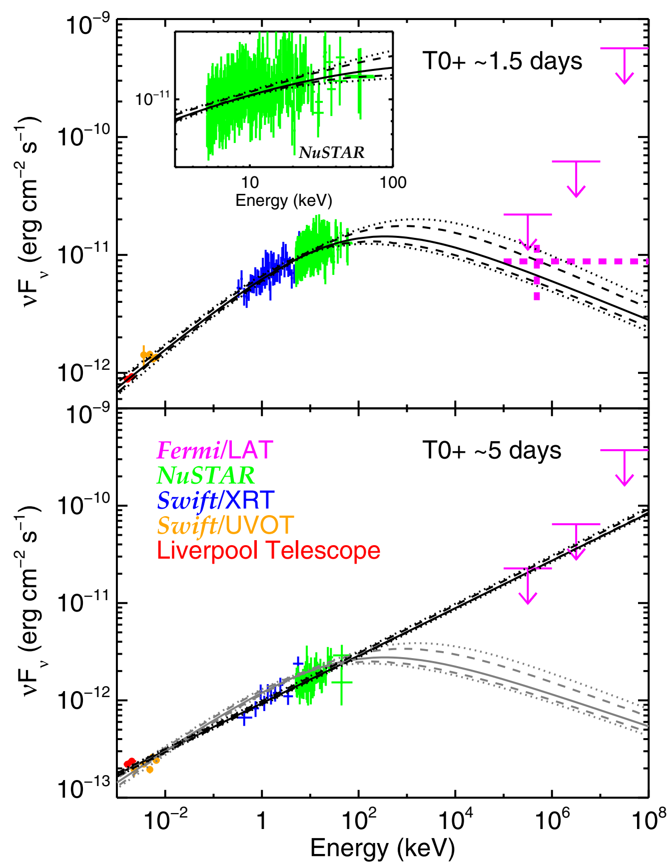

Figure 3. Optical to GeV spectrum of GRB 130427A fit with a SBPL synchrotron model (Granot & Sari 2002). Broadband SEDs are shown during the first (top panel) and the second (bottom panel) *NuSTAR* epochs. The *Fermi*/LAT ULs are shown as arrows and the extrapolation of the LAT flux light curve is shown as a dashed magenta cross (only during the first epoch). The second epoch (bottom panel) is fit with a PL (black line); the fit to the first epoch is scaled down and superposed on the second epoch data for comparison (in gray). The optical/UV/XRT data are corrected for absorption and Galactic extinction. All data point errors are 1σ; the LAT ULs are 2σ; the error contours are 2σ (dashed lines) and 3σ (dotted lines).

(A color version of this figure is available in the online journal.)

NuSTAR epoch started too late for any extrapolation to be meaningful.

Figure 2 exhibits the *Fermi*/LAT photon flux light curve with 1σ confidence intervals derived with such method. We used the same method to compute the flux extrapolation for the first *NuSTAR* epoch (the magenta dashed cross in Figure 3).

4. BROADBAND AFTERGLOW

We extracted light curves and spectra during the *NuSTAR* epochs from *Swift*/UVOT, and *Swift*/XRT using the standard HEASOFT reduction pipelines and the *Swift*/XRT team repository (Evans et al. 2009), as well as Liverpool Telescope data using in-house software (Maselli et al. 2013). For the first epoch, we compare the extrapolation of the LAT temporal and spectral behavior (Ackermann et al. 2013) to our multi-wavelength light curves and spectra.

Figure 3 shows two spectral energy distributions (SEDs) spanning from optical (i' band) to γ-rays (~GeV). We first fit both epochs independently (excluding *Fermi*/LAT data) with two functional forms (Table 1)—single PL and BPL—each multiplied by models for both fixed Galactic and free intrinsic

Table 1
Broadband Spectral Fits during the *NuSTAR* Epochs

Model[1]	Epoch	O+X [2]	N [2]	L [2]	$\Delta\Gamma$ [2]	Γ_1	Γ_2	E_c [2]	χ^2/dof
PL	1	Yes	Yes	...	...	1.72 ± 0.02	...	...	457.6/422[a]
PL	2	Yes	Yes	...	...	1.77 ± 0.02	...	...	105.1/104[b]
BPL	1	Yes	Yes	...	Free	1.70 ± 0.01	$1.89^{+0.08}_{-0.04}$	$9.3^{+2.3}_{-1.4}$	419.3/420[c]
BPL	2	Yes	Yes	...	Free	1.77	...	...	...[d]
BPL	1	Yes	Yes	...	0.5	1.71 ± 0.01	2.21	17 ± 1	428.5/421[e]
BPL	2	Yes	Yes	...	0.5	1.77 ± 0.01	2.27	32^{+14}_{-8}	103.7/103[f]
Fits to Optical+X-ray+*NuSTAR* +LAT confirm presence of break and demonstrate best-fit physical model									
PL	1	Yes	Yes	UL[3]	...	1.72 ± 0.01	...	...	489.1/434[g]
PL[4]	**2**	**Yes**	**Yes**	**UL**[3]	...	$\mathbf{1.76 \pm 0.01}$	...	...	**130.6/116**[a]
BPL	1	Yes	Yes	UL[3]	Free	1.70 ± 0.01	1.91 ± 0.03	$9.4^{+1.4}_{-0.9}$	428.5/432[h]
SBPL	1	Yes	Yes	UL[3]	Free	1.69 ± 0.01	$2.91^{+0.53}_{-0.49}$	96^{+51}_{-25}	422.7/430[i]
SBPL[4]	**1**	**Yes**	**Yes**	**UL**[3]	**0.5**	$\mathbf{1.67 \pm 0.01}$	**2.17**	70^{+59}_{-31}	**427.7/429**[j]

Notes. [1] (PL) power law, (BPL) broken power law, (SBPL) smoothly broken power law. [2]O+X = Optical+*Swift*/XRT + *Swift*/UVOT; N = *NuSTAR*; L = *Fermi*/LAT; $\Delta\Gamma = \Gamma_2 - \Gamma_1$; E_c = break energy in keV. [3]This fit includes the LAT spectra. [4]This spectral fit is shown in Figure 3.
[a] PL is an adequate fit.
[b] PL is an good fit.
[c] BPL is a better fit than PL, F-test = 19.1 ($P = 1.6 \times 10^{-8}$).
[d] Cannot constrain break.
[e] BPL ($\Delta\Gamma = 0.5$) is a better fit than PL, F-test = 28.5 ($P = 1.5 \times 10^{-7}$).
[f] BPL ($\Delta\Gamma = 0.5$) is not significantly better fit than PL, F-test = 1.3 ($P = 0.25$).
[g] PL is not a very good fit.
[h] BPL is a better fit than PL, F-test = 30.5 ($P = 3.9 \times 10^{-13}$), break is needed.
[i] SBPL is a better fit than PL, F-test = 16.9 ($P = 7.2 \times 10^{-13}$).
[j] SBPL is a better fit than PL, F-test = 12.3 ($P = 3.5 \times 10^{-11}$).

(host) extinction (zdust)[17] and absorption (phabs), respectively, and a free cross-calibration constant. We find that both epochs can be fit with a PL; however, the second epoch fit is better ($\chi^2 = 1.01$ versus 1.08 for the first epoch). For the first epoch a BPL is significantly better, with an F-test value of 19.1 (chance probability $P = 1.6 \times 10^{-8}$, see also Table 1).

We then fit the first epoch only with a physically motivated SBPL spectrum described in Granot & Sari (2002), with a fixed sharpness of the break,[18] $s = 0.85$, and including the broadband LAT UL. We performed two fits: (1) keeping the two PL indices free and (2) requiring them to differ by $\Delta\Gamma = 0.5$ according to the synchrotron radiation theoretical expectation (Granot & Sari 2002). The SBPL fit was better (Table 1) and is shown at the top panel of Figure 3, together with the LAT ULs, as well as the extrapolation of the LAT light curve to this epoch; the extrapolation was not used in the fit but plotted for comparison with the model. Both are consistent with the SBPL fit—the curvature in the *NuSTAR* data is also clearly exhibited in the inset in the top panel. The lower panel shows the SED with the second *NuSTAR* epoch fit with a PL and with the first epoch fit shifted and superposed on the plot; although the data do not constrain such a fit, they are consistent with it. Finally, we performed broadband fits removing the *NuSTAR* data (including only optical, *Swift*/XRT, *Swift*/UVOT data, and *Fermi*/LAT ULs) and found that the break energies could not be constrained. Therefore, the *NuSTAR* data are *essential in constraining the shape of the broadband spectra*.

Our results are broadly consistent with those of Perley et al. (2013) who derived radio to GeV afterglow spectra of GRB 130427A covering 0.007–60 days after trigger. Their results also suggest that the forward shock emission indeed dominates at or above the optical during our *NuSTAR* epochs.

5. DISCUSSION

We have shown above that the *NuSTAR* data are consistent with a PL in time and frequency below the cooling-break photon energy E_c, $F_\nu \propto t^{-\alpha}\nu^{-\beta}$ with $\alpha = 1.30 \pm 0.05$ and $\beta \equiv \Gamma_1 - 1 = 0.69 \pm 0.01$ (see Table 1). For the likely PL segment (G from Granot & Sari 2002) of the synchrotron spectrum this implies a PL index of the external medium density, $\rho_{\rm ext} \propto R^{-k}$, where R is the distance from the central source, of $k = 4/[1 + 1/(2\alpha - 3\beta)] = 1.4 \pm 0.2$. Correspondingly, the cooling-break energy scales as $E_c \propto t^{(3k-4)/(8-2k)} = t^{0.05\pm0.12}$, i.e., it is expected to remain constant (which is consistent with our spectral fits, the difference between the two epochs being less than 2σ). The value we obtain for k is intermediate between a uniform interstellar medium ($k = 0$) and a canonical massive-star wind ($k = 2$), possibly indicating that the massive GRB progenitor has produced an eruption (e.g., is opacity driven) prior to its core-collapse, which alters the circumstellar density profile (Fryer et al. 2006). Such an eruption might also account for a variable external density profile, where a transition from a flatter profile to a steeper one might be responsible for the steepening of the optical-to-X-ray light curves after several hours (Ackermann et al. 2013; Laskar et al. 2013). The density profile might have been relatively steep ($k \sim 1$–2) during the first few hundred seconds, shortly after the outflow deceleration time, possibly accounting for the early reverse shock emission (Laskar et al. 2013; Perley et al. 2013).

The *NuSTAR* PL distributions in time and frequency support an afterglow synchrotron origin (Kumar & Barniol Duran 2009, 2010; Ghisellini et al. 2010). Synchrotron radiation models

[17] The Small Magellanic Cloud extinction curve fits our data best and we use it exclusively for continuity.
[18] This value corresponds to the cooling break for our inferred photon index and external density profile (Granot & Sari 2002).

predict a maximum synchrotron photon energy, $E_{\rm syn,max}$, derived by equating the electron acceleration and synchrotron radiative cooling timescales, assuming a single acceleration and emission region (Guilbert et al. 1983; de Jager et al. 1996; Kirk & Reville 2010; Piran & Nakar 2010). In the context of late-time *Fermi*/LAT high-energy photons, this was first briefly mentioned as a problem for a synchrotron origin for GRB 090902B (Abdo et al. 2009), and later discussed more generally and in depth by Piran & Nakar (2010). The long-lasting ($\sim$1 day) *Fermi*/LAT afterglow included a 32 GeV photon after 34 ks, and altogether five >30 GeV photons after >200 s. All five significantly exceed $E_{\rm syn,max}$, by factors of 6.25 for $k = 0$ and 9.20 for $k = 2$ (using Equation (4) of Piran & Nakar 2010). This led to suggestions that the *Fermi*/LAT high-energy photons were not synchrotron radiation, but instead arose from a distinct high-energy spectral component (Ackermann et al. 2013; Fan et al. 2013).

Such a component may arise, for example, from synchrotron self-Compton (Fan et al. 2013). This mechanism was predicted to dominate at high photon energies at late times (Panaitescu & Kumar 2000; Sari & Esin 2001), but has rarely been detected in the late X-ray afterglow (Harrison et al. 2001; Yost et al. 2002). Other possible origins of the high-energy emission involve long-lived activity of the central source, producing a late relativistic outflow that provides seed synchrotron photons or relativistic electrons that might scatter either their own synchrotron emission or that of the afterglow shock (Fan & Piran 2008). In GRB 130427A, however, there are no signs of prolonged central source activity (such as X-ray flares) beyond hundreds of seconds. Another option is a "pair echo" involving TeV photons emitted promptly by the GRB, which pair-produce with photons of the extragalactic background light; for low enough intergalactic magnetic fields the resulting pairs can produce detectable longer-lived GeV emission by upscattering cosmic microwave background photons (Plaga 1995; Takahashi et al. 2008). However, in this case the flux decay rate is expected to gradually steepen and the photon index to soften, in contrast with observations. A different possibility is pair cascades, induced by shock-accelerated ultra-high-energy cosmic rays (Dermer & Atoyan 2006).

For any of these alternative models to work, there needs to be a transition from synchrotron emission (at low photon energies) to the alternative model (at high energies). We expect that if a distinct spectral component dominated the emission at GeV energies, it would naturally show up in a broadband SED. By combining optical, XRT, *NuSTAR*, and *Fermi*/LAT UL data we have shown that the SED at $\sim$1.5 days is perfectly consistent with the theoretically expected SBPL spectral shape from optical to GeV energies, without any unaccounted for flux, and that the flux at all these energies decays at a similar rate. This strongly suggests a single underlying spectral component over a wide energy range. For low energies, the most viable emission mechanism for such a spectral component is synchrotron radiation, suggesting that the entire SED is produced by synchrotron emission.

Therefore, our results strongly suggest that the late-time *Fermi*/LAT high-energy photons in GRB 130427A are indeed afterglow synchrotron radiation, and provide the strongest direct observational support to date for such an afterglow synchrotron origin of late-time >10 GeV *Fermi*/LAT photons. As was already pointed out (e.g., Piran & Nakar 2010), such an origin challenges particle acceleration models in afterglow shocks. In particular, at least one of the assumptions in estimating $E_{\rm syn,max}$ must be incorrect, requiring a modification of our understanding of afterglow shock physics. While many authors were aware of this potential problem, the *NuSTAR* results make it much harder to circumvent. One possible solution may lie in changing the assumption of a uniform magnetic field into a lower magnetic field acceleration region and a higher magnetic field synchrotron radiation region (Kumar et al. 2012; Lyutikov 2010). These might arise for diffusive shock acceleration (Fermi Type I) if the tangled shock-amplified magnetic field decays on a short length scale behind the shock front (where most of the high-energy radiation is emitted), while the highest energy electrons are accelerated in the lower magnetic field further downstream (Kumar et al. 2012).

Another possibility is direct linear acceleration in the electric field of magnetic reconnection layers, which have a low magnetic field (Uzdensky et al. 2011; Cerutti et al. 2012, 2013). This would require, however, a significant fraction of the total energy in the flow to reside in magnetic fields of alternating sign. This is not expected in GRB afterglows, but it could occur in the magnetic-reconnection induced decay of the tangled shock-amplified field mentioned above, which initially reaches near-equipartition values just behind the shock. While the exact solution is still unclear, our results provide an important challenge for our understanding of particle acceleration and magnetic field amplification in relativistic shocks.

This work was supported under NASA Contract NNG08FD60C, and made use of data from the *NuSTAR* mission, a project led by CalTech, managed by JPL, and funded by NASA. We thank the *NuSTAR* Operations, Software and Calibration teams for support with the execution and analysis of these observations. This research has made use of the *NuSTAR* Data Analysis Software (NuSTARDAS) jointly developed by the ASI Science Data Center (ASDC, Italy) and CalTech. This work made use of data supplied by the UK *Swift* Science Data Centre at the University of Leicester. The *Fermi*/LAT Collaboration acknowledges support from NASA and DOE (U.S.), CEA/Irfu and IN2P3/CNRS (France), ASI and INFN (Italy), MEXT, KEK, and JAXA (Japan), and the K.A. Wallenberg Foundation, the Swedish Research Council and the National Space Board in Sweden. Additional support from INAF in Italy and CNES in France for science analysis during the operations phase is also gratefully acknowledged. The Liverpool Telescope is operated by Liverpool John Moores University at the Observatorio del Roque de los Muchachos of the Instituto de Astrofisica de Canarias. C.G.M. acknowledges support from the Royal Society.

REFERENCES

Abdo, A. A., Ackermann, M., Ajello, M., et al. 2009, ApJL, 706, L138
Ackermann, M., Ajello, M., Asano, K., et al. 2013, Sci, in press
Ackermann, M., Albert, A., Baldini, L., et al. 2012, ApJ, 754, 121
Cerutti, B., Uzdensky, D., & Begelman, M. C. 2012, ApJ, 746, 148
Cerutti, B., Werner, G. R., Uzdensky, D. A., & Begelman, M. C. 2013, ApJ, 770, 147
Covino, S., Ghisellini, G., Lazzati, D., & Malesani, D. 2004, in ASP Conf. Ser. 312, Third Rome Workshop on Gamma-Ray Bursts in the Afterglow Era, ed. M. Feroci, F. Frontera, N. Masetti, & L. Piro (San Francisco, CA: ASP), 169
de Jager, O. C., Harding, A. K., Michelson, P. F., et al. 1996, ApJ, 457, 253
Dermer, C., & Atoyan, A. 2006, NJPh, 8, 122
Evans, P. A., Beardmore, A. P., Page, K. L., et al. 2009, MNRAS, 397, 1177
Fan, Y.-Z., & Piran, T. 2008, FrPhC, 3, 306
Fan, Y.-Z., Tam, P. H. T., Zhang, F.-W., et al. 2013, ApJ, 776, 95
Fryer, C. L., Rockefeller, G., & Young, P. A. 2006, ApJ, 647, 1269
Galama, T. J., Wijers, R. A. M. J., Bremer, M., et al. 1998, ApJ, 500, L97

Ghisellini, G., Ghirlanda, G., Nava, L., & Celotti, A. 2010, MNRAS, 403, 926
Golenetskii, S., Aptekar, R., Frederiks, D., et al. 2013, GCN Circ., 14487
Goodman, J., & Weare, J. 2010, Commun. Appl. Math. Comput. Sci., 5.1, 65
Granot, J., & Sari, R. 2002, ApJ, 568, 820
Guilbert, P. W., Fabian, A. C., & Rees, M. J. 1983, MNRAS, 205, 593
Harrison, F. A., Craig, W. W., Christensen, F. E., et al. 2013, ApJ, 770, 103
Harrison, F. A., Yost, S. A., Sari, R., et al. 2001, ApJ, 559, 123
Kirk, J. G., & Reville, B. 2010, ApJL, 710, L16
Kouveliotou, C., Wijers, R. A. M. J., & Woosley, S. E. 2012, Gamma-Ray Bursts (Cambridge: Cambridge Univ. Press)
Kumar, P., & Barniol Duran, R. 2009, MNRAS, 400, L75
Kumar, P., & Barniol Duran, R. 2010, MNRAS, 409, 226
Kumar, P., Hernández, R. A., Bosnjak, Z., & Barniol Duran, R. 2012, MNRAS, 427, L40
Laskar, T., Berger, E., Zauderer, B. A., et al. 2013, ApJ, 776, 119
Levan, A., Cenko, S. B., Perley, D. A., & Tanvir, N. R. 2013, GCN Circ., 14455
Lyutikov, M. 2010, MNRAS, 405, 1809
Maselli, A., Beardmore, A. P., Lien, A. Y., et al. 2013, GCN Circ., 14448
Maselli, A., Melandri, A., Nava, L., et al. 2013, Sci, in press
Nolan, P. L., Abdo, A. A., Ackermann, M., et al. 2012, ApJS, 199, 31
Panaitescu, A., & Kumar, P. 2000, ApJ, 543, 66
Perley, D. A., et al. 2013, ApJ, submitted (arXiv:1307.4401)
Piran, T., & Nakar, E. 2010, ApJL, 718, L63
Plaga, R. 1995, Natur, 374, 430
Preece, R., Burgess, J. M., von Kienlin, A., et al. 2013, Sci, in press
Sari, R., & Esin, A. A. 2001, ApJ, 548, 787
Smith, G. M., Csillaghy, A., Hurley, K., et al. 2013, GCN Circ., 14590
Takahashi, K., Murase, K., Ichiki, K., Inoue, S., & Nagataki, S. 2008, ApJL, 687, L5
Uzdensky, D., Cerutti, B., & Begelman, M. C. 2011, ApJL, 737, L40
Verrecchia, F., Pittori, C., Giuliani, A., et al. 2013, GCN Circ., 14515
von Kienlin, A. 2013, GCN Circ., 14473
Yost, S. A., Frail, D. A., Harrison, F. A., et al. 2002, ApJ, 577, 155